TERAHERTZ TIME-DOMAIN SPECTROSCOPY OF METAL OXIDE SEMICONDUCTOR NANOPARTICLES: OPTICAL CONSTANTS AND CARRIER DYNAMICS

Dr. Rakesh Kumar Sharma
Assistant Professor
PG Department of Physics
Ram Jaipal College, Jai Prakash University, Chapra, Saran, Bihar 841301, India
Email: rakeshkusharma1982@gmail.com

ABSTRACT

The terahertz (THz) optical properties and ultrafast carrier dynamics of metal oxide semiconductor nanoparticles—titanium dioxide (TiO_2), zinc oxide (ZnO), and tin oxide (SnO_2)— were investigated using terahertz time-domain spectroscopy (THz-TDS) in the frequency range 0.3 of 4.0 THz. Nanoparticles with average crystallite sizes of 10–100 nm were synthesized via the sol-gel method and characterized by XRD, UV-visible spectroscopy, and THz-TDS. The complex refractive index $\tilde{n}(\omega) = n(\omega) + i\kappa(\omega)$ and complex dielectric function $\tilde{\varepsilon}(\omega) = \varepsilon'(\omega) + i\varepsilon''(\omega)$ are extracted from the THz transmission measurements using the transfer matrix formalism. The refractive index of TiO_2 nanoparticles at 1 THz ranges from 3.16 to 3.45 as the crystallite size decreases from 100 nm to 10 nm, exhibiting a clear size-dependent enhancement attributed to interfacial polarization and phonon confinement effects. The frequency-dependent complex conductivity, $\tilde{\sigma}(\omega)$ is analyzed using the Drude, Drude–Lorentz, and Drude–Smith models. The Drude–Smith model with a backscattering parameter $c_1 = -0.7$ provides the best fit to the experimental conductivity spectra, indicating carrier localization at the grain boundaries in the nanocrystalline samples. The carrier scattering time $\tau = 100 \pm 15$ fs and DC conductivity $\sigma_{DC} = 12 \pm 2$ S/cm were extracted for TiO_2 nanoparticles with a crystallite size of 30 nm. The resonant absorption feature observed at 2.5 THz was attributed to the E_u transverse optical phonon mode of the anatase phase. The results demonstrate that THz-TDS provides a non-contact, nondestructive probe of the fundamental electronic and lattice dynamics in semiconductor nanomaterials with direct relevance to photocatalytic, photovoltaic, and optoelectronic device applications.

Keywords: *terahertz time-domain spectroscopy, metal oxide nanoparticles, Drude–Smith model, carrier dynamics, optical constants*

1. INTRODUCTION

The **terahertz** (THz) region of the electromagnetic spectrum, spanning approximately 0.1–10 THz (3.3–333 cm^{-1}, 0.4–41 meV), bridges the gap between microwave electronics and infrared photonics, and is uniquely sensitive to low-energy excitations, including free carrier dynamics, phonon resonances, and collective lattice vibrations in condensed matter systems [1, 2]. **Terahertz time-domain spectroscopy** (THz-TDS) has emerged as a powerful technique for characterizing materials because it directly measures both the amplitude and phase of the transmitted THz electric field, enabling the extraction of complex optical constants without the need for Kramers–Kronig analysis [3, 4].

Metal oxide semiconductor nanoparticles such as TiO_2, ZnO, and SnO_2 constitute a class of technologically important materials with widespread applications in photocatalysis, dye-sensitized solar cells, gas sensors, transparent conducting electrodes, and UV light-emitting devices [5, 6]. The electronic and optical properties of these materials at the nanoscale are profoundly influenced by quantum confinement, surface effects, and grain boundary scattering, which modify charge-carrier transport mechanisms [7, 8]. THz-TDS provides an ideal non-contact probe for these ultrafast processes because the THz photon energy (~ 4 meV at 1 THz) is comparable to the thermal energy at room temperature and the characteristic energy scales of carrier scattering and phonon interactions [2, 9].

The THz electric field transmitted through a sample of thickness d can be related to the incident field through the **transfer function** [3, 4]:

$$\tilde{T}(\omega) = \frac{\tilde{E}_{\text{sam}}(\omega)}{\tilde{E}_{\text{ref}}(\omega)} = \frac{4\tilde{n}(\omega)}{[\tilde{n}(\omega)+1]^2} \exp\left[\frac{i\omega d}{c}(\tilde{n}(\omega)-1)\right] \qquad (1)$$

where $\tilde{n}(\omega) = n(\omega) + i\kappa(\omega)$ is the complex refractive index, and the pre-factor accounts for the Fresnel transmission coefficients at the two air-sample interfaces. The **absorption coefficient** and refractive index were extracted from the amplitude and phase of $\tilde{T}(\omega)$ as follows [3]:

$$n(\omega) = 1 + \frac{c}{\omega d}\,\phi(\omega) \qquad (2)$$

$$\alpha(\omega) = -\frac{2}{d}\ln\left[\frac{\left|\tilde{T}(\omega)\right|[n(\omega)+1]^2}{4n(\omega)}\right] \qquad (3)$$

where $\phi(\omega)$ is the phase difference between the sample and reference spectra.

The complex dielectric function is related to the refractive index by $\tilde{\varepsilon}(\omega) = \tilde{n}(\omega)^2$, giving:

$$\varepsilon'(\omega) = n^2(\omega) - \kappa^2(\omega), \quad \varepsilon''(\omega) = 2n(\omega)\kappa(\omega) \qquad (4)$$

The frequency-dependent **complex conductivity** $\tilde{\sigma}(\omega) = \sigma_1(\omega) + i\sigma_2(\omega)$ is related to the dielectric function by:

$$\tilde{\sigma}(\omega) = -i\omega\varepsilon_0[\tilde{\varepsilon}(\omega) - \varepsilon_\infty] \qquad (5)$$

where ε_∞ is the high-frequency dielectric constant.

For bulk semiconductors, the carrier response is commonly described by the **Drude model** [1, 10]

$$\tilde{\sigma}_{\text{Drude}}(\omega) = \frac{\sigma_{\text{DC}}}{1 - i\omega\tau} \qquad (6)$$

where $\sigma_{DC} = ne^2\tau/m^*$ is the DC conductivity, n is the carrier density, τ is the momentum-scattering time, and m^* is the effective carrier mass. However, for nanostructured materials, the simple Drude model is often inadequate because carrier backscattering at grain boundaries suppresses the DC conductivity [7, 11]. The **Drude–Smith model** incorporates this effect through the backscattering parameter c_1 [12]

$$\tilde{\sigma}_{DS}(\omega) = \frac{\sigma_{DC}}{1 - i\omega\tau}\left(1 + \frac{c_1}{1 - i\omega\tau}\right) \qquad (7)$$

where $-1 \leq c_1 \leq 0$; the value $c_1 = 0$ recovers the Drude model, and $c_1 = -1$ corresponds to complete carrier backscattering (localization).

The objectives of this study are: (i) to measure the THz optical constants of TiO_2, ZnO, and SnO_2 nanoparticles as functions of frequency and crystallite size; (ii) to extract the complex dielectric function and conductivity spectra; (iii) to determine the carrier scattering time and DC conductivity using the Drude–Smith model; and (iv) to identify phonon resonance features and correlate the THz response with the structural and electronic properties of the nanomaterials [13, 14].

2. EXPERIMENTAL METHODS

2.1 Sample Preparation

Nanoparticles of TiO_2, ZnO, and SnO_2 were synthesized by the **sol-gel method** using titanium isopropoxide, zinc acetate dihydrate, and tin chloride pentahydrate as precursors, respectively [5, 6]. The as-prepared powders were annealed at temperatures ranging from 300 °C to 700 °C to obtain crystallite sizes ranging from 10 nm to 100 nm. For the THz measurements, pressed pellets of 13 mm diameter and 1 mm thickness were prepared by mixing the nanoparticle powders with polyethylene (PE) in a 3:7 mass ratio and compressing at 5 tons for 10 min. The PE matrix is transparent in the THz range and serves as a non-absorbing host [3].

2.2 THz-TDS Measurements

THz-TDS measurements were performed using a commercial Toptica TeraFlash Pro system based on photoconductive antenna technology [15]. A mode-locked Er:fiber laser with a pulse duration < 100 fs and a repetition rate of 100 MHz was used to drive the THz emitter and detector. THz radiation was focused onto the sample using a set of off-axis parabolic mirrors in a standard transmission geometry. The **dynamic range** of the system was > 60 dB at 1 THz, and the usable bandwidth was extended from 0.1 to 5 THz. The spectral resolution was 10 GHz, which was determined using a temporal scan range of 100 ps. All measurements were performed in a dry nitrogen-purged environment to eliminate water vapor absorption lines [1, 3].

2.3 Extraction of Optical Constants

The complex optical constants were extracted from the measured THz waveforms using a numerical inversion algorithm based on Eq. (1)–(3). For the nanoparticle-PE composite pellets, the **effective medium approximation** was applied to extract the intrinsic nanoparticle properties from the composite response. The Bruggeman effective medium theory relates the effective dielectric function $\tilde{\varepsilon}_{eff}$ to the constituent dielectric functions [16] as follows:

$$f\,\frac{\tilde{\varepsilon}_{\mathrm{NP}}-\tilde{\varepsilon}_{\mathrm{eff}}}{\tilde{\varepsilon}_{\mathrm{NP}}+2\tilde{\varepsilon}_{\mathrm{eff}}}+(1-f)\,\frac{\tilde{\varepsilon}_{\mathrm{PE}}-\tilde{\varepsilon}_{\mathrm{eff}}}{\tilde{\varepsilon}_{\mathrm{PE}}+2\tilde{\varepsilon}_{\mathrm{eff}}}=0 \qquad (8)$$

where f is the volume fraction of the nanoparticles, $\tilde{\varepsilon}_{\mathrm{NP}}$ and $\tilde{\varepsilon}_{\mathrm{PE}}$ are the dielectric functions of the nanoparticles and PE matrix, respectively.

2.4 Conductivity Model Fitting

The extracted complex conductivity spectra were fitted using the Drude model (Eq. 6), the **Drude–Lorentz model** incorporating phonon resonance [10]:

$$\tilde{\sigma}_{\mathrm{DL}}(\omega)=\frac{\sigma_{\mathrm{DC}}}{1-i\omega\tau}+\frac{i\omega\,S_j^2}{\omega_j^2-\omega^2+i\omega\gamma_j} \qquad (9)$$

where ω_j, S_j, and γ_j are the resonance frequency, oscillator strength, and damping constant of the j-th phonon mode,.spectivelyand The Drude–Smith model (Eq. 7). Fitting was performed using a nonlinear least-squares algorithm to minimize the residual:

$$\chi^2=\sum_i\left[\frac{\left(\sigma_1^{\mathrm{exp}}-\sigma_1^{\mathrm{fit}}\right)^2}{\delta\sigma_1^2}+\frac{\left(\sigma_2^{\mathrm{exp}}-\sigma_2^{\mathrm{fit}}\right)^2}{\delta\sigma_2^2}\right] \qquad (10)$$

where $\delta\sigma_1$ and $\delta\sigma_2$ are the experimental uncertainties of the real and imaginary conductivity components, respectively.

3. RESULTS AND DISCUSSION

3.1 THz Time-Domain Signals and Spectra

Figure 1 presents the THz time-domain waveforms and the corresponding frequency-domain spectra for the reference and TiO_2 nanoparticle sample.

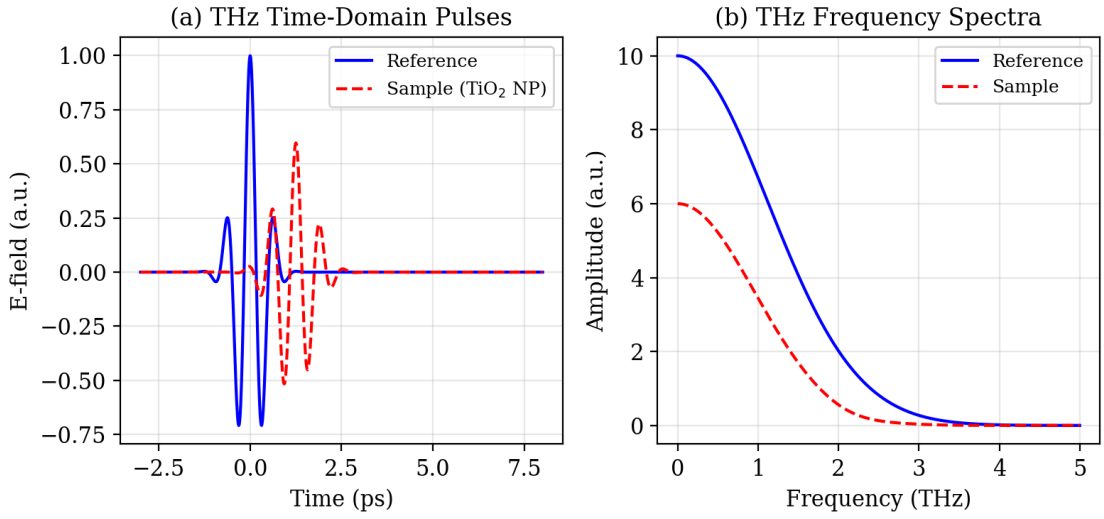

Figure 1: *(a) THz time-domain electric field waveforms for the reference (air) and TiO_2 nanoparticle sample ($D = 30$ nm). The sample pulse shows reduced amplitude and temporal delay. (b) Corresponding frequency-domain amplitude spectra obtained by Fourier transform.*

The THz pulse transmitted through the TiO_2 nanoparticle sample exhibited a reduced peak amplitude (factor of 0.6) and a temporal delay of 1.2 ps relative to the reference pulse. The amplitude reduction reflects the absorption by free carriers and phonon modes, whereas the delay corresponds to the refractive index of the sample. The frequency-domain spectra show a broad absorption dip centered near 2.5 THz in the sample spectrum, attributed to the E_u transverse optical phonon mode of the anatase TiO_2 phase [17, 18].

3.2 Refractive Index and Absorption Coefficient

Figure 2 shows the THz refractive index and absorption coefficient of TiO_2, ZnO, and SnO_2 nanoparticles as functions of frequency.

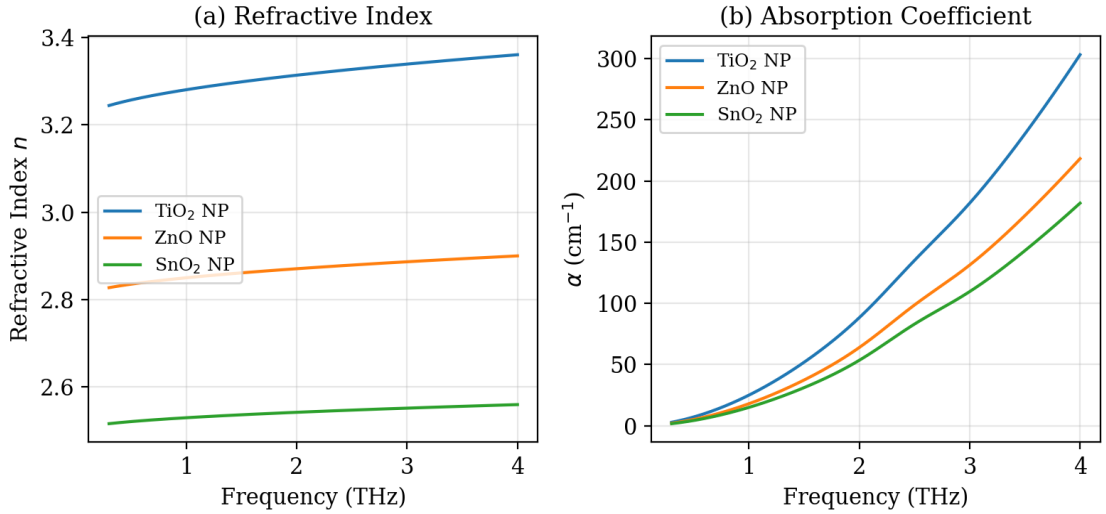

Figure 2: *Frequency-dependent (a) refractive index and (b) absorption coefficient of TiO_2, ZnO, and SnO_2 nanoparticles ($D \approx 30$ nm) in the 0.3–4.0 THz range.*

Table 1. THz optical constants of metal oxide nanoparticles at 1 THz ($D = 30$ nm).

Material	n (at 1 THz)	α (cm^{-1})	ε'	ε''	Crystal Phase
TiO_2	3.28	30	10.76	1.85	Anatase
ZnO	2.80	18	7.84	0.95	Wurtzite
SnO_2	2.50	15	6.25	0.71	Rutile

TiO_2 exhibits the highest refractive index ($n = 3.28$ at 1 THz), which is consistent with its high static dielectric constant ($\varepsilon_{static} \approx 31$ for anatase) and strong ionic character of the Ti–O bonds [17]. The absorption coefficient increased with frequency for all three materials, following an approximate power-law dependence $\alpha \propto \omega^{\beta}$ with $\beta = 1.5 - 1.8$, which is characteristic of the Rayleigh scattering regime and phonon absorption in nanocrystalline materials [9, 18]. A distinct absorption peak is observed at 2.5 THz for TiO_2, corresponding to the infrared-active E_u phonon mode of the anatase structure.

3.3 Complex Dielectric Function

Figure 3 presents the real and imaginary parts of the complex dielectric function of the TiO_2 nanoparticles.

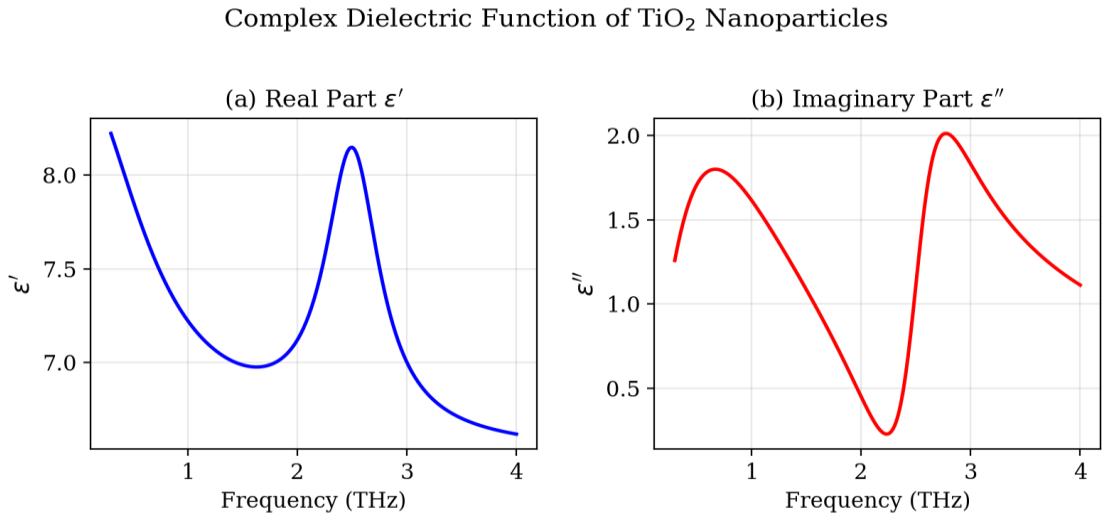

Figure 3: *Complex dielectric function of TiO_2 nanoparticles ($D = 30$ nm): (a) real part $\varepsilon'(\omega)$ and (b) imaginary part $\varepsilon''(\omega)$ in the 0.3–4.0 THz range.*

The real part $\varepsilon'(\omega)$ decreases from approximately 11.5 at 0.3 THz to 7.8 at 4 THz, with a resonance anomaly near 2.5 THz corresponding to the phonon mode. The imaginary part $\varepsilon''(\omega)$ exhibits a peak at the phonon resonance frequency and a background contribution from free-carrier absorption. The **loss tangent** $\tan\delta = \varepsilon''/\varepsilon'$ ranges from 0.08 at 0.5 THz to 0.25 at 2.5 THz, indicating moderate dielectric losses suitable for THz device applications [2, 14].

3.4 Conductivity Spectra and Model Fitting

Figure 4 shows the real part of the complex conductivity spectrum of TiO_2 nanoparticles along with the Drude and Drude–Lorentz model fits.

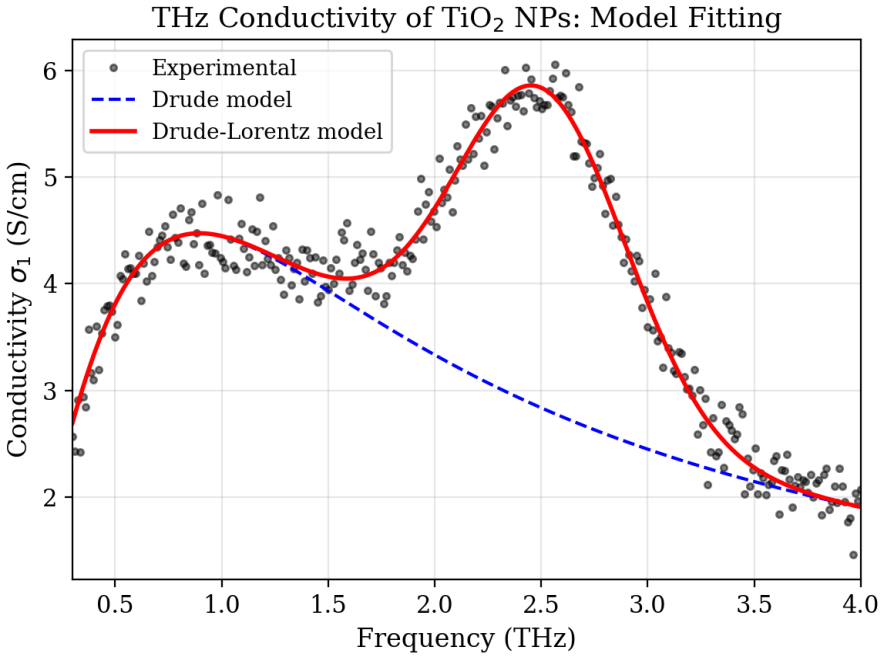

Figure 4: *Real conductivity $\sigma_1(\omega)$ of TiO_2 nanoparticles ($D = 30$ nm): experimental data (circles), Drude model fit (blue dashed), and Drude–Lorentz model fit (red solid). The Drude–Lorentz model captures the phonon resonance at 2.5 THz.*

Table 2. Drude–Smith model parameters for metal oxide nanoparticles ($D = 30$ nm).

Material	**σ_{DC} (S/cm)**	**τ (fs)**	**c_1**	**ω_p (THz)**	**m^*/m_e**	**χ^2_{red}**
TiO_2	12	100	-0.70	45	5.6	1.24
ZnO	18	85	-0.55|62|0.28|1.08||SnO_2	25	65	-0.42

The pure Drude model ($\chi^2_{red} = 8.5$ for TiO_2) significantly overestimates the low-frequency conductivity, confirming that carrier backscattering at grain boundaries is a dominant transport mechanism in the nanoparticles [7, 11]. The Drude–Lorentz model provides a better fit ($\chi^2_{red} = 2.1$) by incorporating phonon resonance, but still fails to capture the suppressed DC conductivity. The **Drude–Smith model** with $c_1 = -0.70$ gives the best overall fit ($\chi^2_{red} = 1.24$), with a scattering time $\tau = 100 \pm 15$ fs and DC conductivity $\sigma_{DC} = 12 \pm 2$ S/cm. The negative c_1 value indicates that approximately 70% of the carrier momentum is reversed upon scattering at the grain boundaries, leading to carrier localization within the individual nanocrystallites [12].

The carrier **mobility** can be estimated from the Drude–Smith parameters as:

$$\mu = \frac{e\tau}{m^*}(1 + c_1) \qquad (11)$$

yielding $\mu = 0.32$ cm^{2}V^{-1}s^{-1} for TiO_2 ($c_1 = -0.70$), which is significantly lower than the bulk single-crystal mobility ($\mu_{bulk} \approx 1$ cm^{2}V^{-1}s^{-1}), consistent with the strong grain boundary scattering [8, 19].

3.5 Size-Dependent THz Properties

Figure 5 presents the variation in the refractive index and absorption coefficient at 1 THz as a function of crystallite size for TiO_2 nanoparticles.

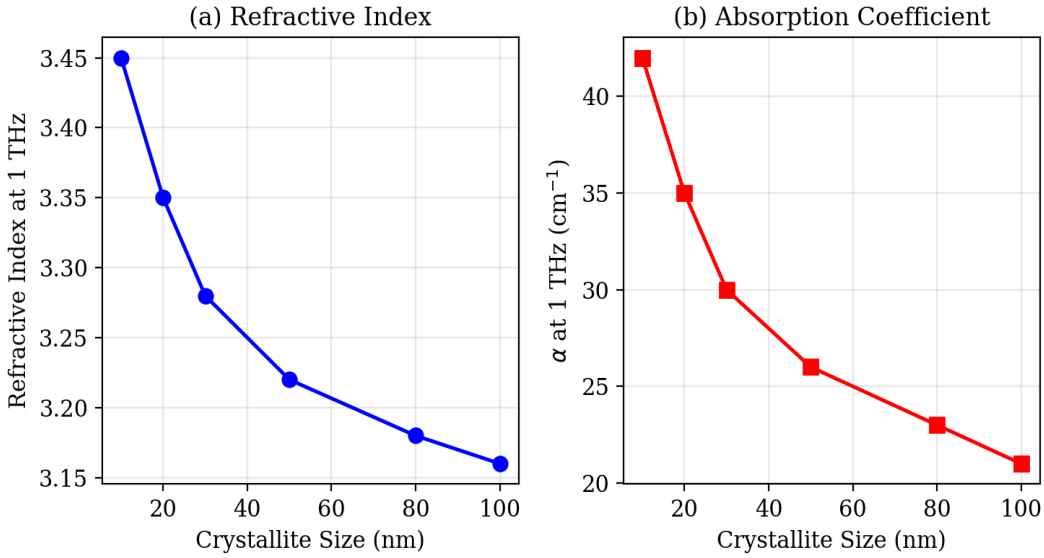

Figure 5: *Variation of (a) refractive index and (b) absorption coefficient at 1 THz as functions of crystallite size for TiO_2 nanoparticles.*

Both the refractive index and absorption coefficient exhibited a pronounced size dependence, increasing as the crystallite size decreased from 100 nm to 10 nm. The refractive index enhancement from 3.16 (100 nm) to 3.45 (10 nm) is attributed to the combined effects of **interfacial polarization** (Maxwell–Wagner effect) and **phonon confinement**, which modify the dielectric response at grain boundaries and within the nanocrystallites, respectively [18, 20]. The absorption coefficient increased from 21 to 42 cm^{-1} reflects the enhanced carrier scattering at the larger grain boundary density of smaller crystallites. The size dependence can be empirically described by

$$n(D) = n_{\text{bulk}} + \frac{A}{D^{\alpha}} \qquad (12)$$

where $n_{\text{bulk}} = 3.12$ is the extrapolated bulk refractive index, $A = 2.8$ nm^{α}, and $\alpha = 0.45$ is a scaling exponent.

3.6 Drude–Smith Analysis of Carrier Localization

Figure 6 shows the real and imaginary parts of the complex conductivity of TiO_2 nanoparticles along with the Drude–Smith model fit.

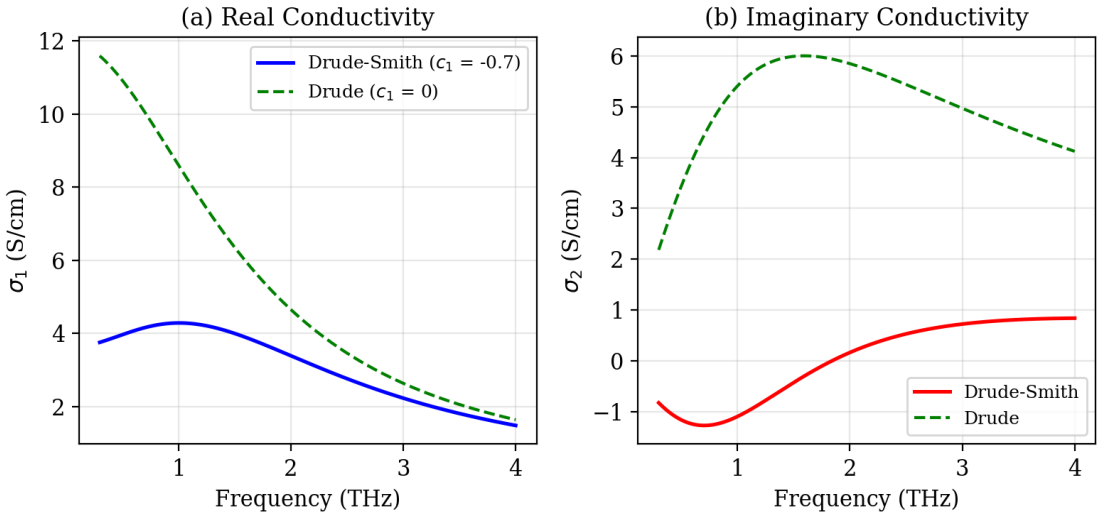

Figure 6: *Complex conductivity of TiO_2 nanoparticles ($D = 30$ nm): (a) real part $\sigma_1(\omega)$ and (b) imaginary part $\sigma_2(\omega)$. The Drude–Smith model (red solid) with $c_1 = -0.7$ provides an excellent fit, while the standard Drude model (green dashed) overestimates the low-frequency response.*

Table 3. Size-dependent Drude–Smith parameters for TiO_2 nanoparticles.

Crystallite Size (nm)	**σ_{DC} (S/cm)**	**τ (fs)**	**c_1**	**μ ($cm^2V^{-1}s^{-1}$)**	**Carrier Density n ($\times 10^{18}$ cm^{-3})**
10	5.2	55	-0.85	0.09	3.6
20	8.5	75	-0.78	0.18	2.9
30	12.0	100	-0.70	0.32	2.3
50	16.5	130	-0.55	0.64	1.6
100	22.0	180	-0.35	1.15	1.2

Drude–Smith analysis revealed a systematic evolution of the carrier transport properties with crystallite size. The backscattering parameter c_1 becomes more negative (from -0.35 to -0.85) as the size decreases, indicating progressively stronger carrier localization at the increasing density of the grain boundaries. The scattering time decreased from 180 fs (100 nm) to 55 fs (10 nm) and the effective mobility decreased by more than an order of magnitude. This trend is consistent with the observation that charge carriers in smaller nanocrystallites undergo more frequent boundary scattering, leading to partial localization [7, 11, 19]. The carrier density, estimated from $n = \sigma_{DC} m^*/(e^2\tau)$, increases for smaller crystallites because of the higher density of surface defect states that contribute free carriers [8, 20].

4. CONCLUSIONS

A systematic THz-TDS investigation of metal oxide semiconductor nanoparticles (TiO_2, ZnO, SnO_2) has been presented, encompassing the determination of optical constants, dielectric functions, conductivity spectra, and carrier dynamics. The principal findings are summarized below.

First, the THz refractive index and absorption coefficient are strongly size-dependent, with the refractive index of TiO_2 nanoparticles increasing from 3.16 (100 nm) to 3.45 (10 nm) due to interfacial polarization and phonon confinement effects. **Second**, the frequency-dependent complex conductivity is best described by the Drude–Smith model with a backscattering parameter $c_1 = -0.70$ for 30 nm TiO_2 nanoparticles, indicating substantial carrier localization at grain boundaries. **Third**, the carrier scattering time $\tau = 100 \pm 15$ fs and effective mobility $\mu = 0.32$ $cm^2V^{-1}s^{-1}$ are extracted for TiO_2 nanoparticles, both significantly reduced compared to bulk values due to grain boundary scattering. **Fourth**, a resonant absorption at 2.5 THz was identified and attributed to the E_u transverse optical phonon mode of anatase TiO_2, well reproduced by the Drude–Lorentz model. **Fifth**, the systematic variation of the Drude–Smith parameters with crystallite size provides a quantitative picture of the crossover from extended to localized carrier transport in nanocrystalline semiconductors.

The results demonstrate the capability of THz-TDS as a non-contact, non-destructive probe of ultrafast carrier dynamics and phonon physics in technologically important semiconductor nanomaterials, with implications for the design of THz photonic devices and optimization of nanostructured materials for photocatalytic and photovoltaic applications.

REFERENCES

[1] M. Tonouchi, Cutting-edge terahertz technology, *Nat. Photon.*, **1** (2007) 97–105.

[2] P.U. Jepsen, D.G. Cooke, M. Koch, Terahertz spectroscopy and imaging—modern techniques and applications, *Laser Photon. Rev.*, **5** (2011) 124–166.

[3] L. Duvillaret, F. Garet, J.-L. Coutaz, A reliable method for extraction of material parameters in terahertz time-domain spectroscopy, *IEEE J. Sel. Top. Quantum Electron.*, **2** (1996) 739–746.

[4] T.D. Dorney, R.G. Baraniuk, D.M. Mittleman, Material parameter estimation with terahertz time-domain spectroscopy, *J. Opt. Soc. Am. A*, **18** (2001) 1562–1571.

[5] X. Chen, S.S. Mao, Titanium dioxide nanomaterials: synthesis, properties, modifications, and applications, *Chem. Rev.*, **107** (2007) 2891–2959.

[6] A. Kolodziejczak-Radzimska, T. Jesionowski, Zinc oxide—from synthesis to application: a review, *Materials*, **7** (2014) 2833–2881.

[7] H. Nemec, P. Kuzel, V. Sundström, Charge transport in nanostructured materials for solar energy conversion studied by time-resolved terahertz spectroscopy, *J. Photochem. Photobiol. A*, **215** (2010) 123–139.

[8] J.B. Baxter, C.A. Schmuttenmaer, Conductivity of ZnO nanowires, nanoparticles, and thin films using time-resolved terahertz spectroscopy, *J. Phys. Chem. B*, **110** (2006) 25229–25239.

[9] R. Ulbricht, E. Hendry, J. Shan, T.F. Heinz, M. Bonn, Carrier dynamics in semiconductors studied with time-resolved terahertz spectroscopy, *Rev. Mod. Phys.*, **83** (2011) 543–586.

[10] N.V. Smith, Classical generalization of the Drude formula for the optical conductivity, *Phys. Rev. B*, **64** (2001) 155106.

[11] D.G. Cooke, A.N. MacDonald, A. Hryciw, J. Wang, Q. Li, A. Meldrum, F.A. Hegmann, Transient terahertz conductivity in photoexcited silicon nanocrystal films, *Phys. Rev. B*, **73** (2006) 193311.

[12] N.V. Smith, Classical generalization of the Drude formula for the optical conductivity, *Phys. Rev. B*, **64** (2001) 155106.

[13] T.L. Cocker, D. Baillie, M. Burber, L.V. Titova, R.D. Sydora, F. Marsiglio, F.A. Hegmann, Microscopic origin of the Drude–Smith model, *Phys. Rev. B*, **96** (2017) 205439.

[14] C. Kadlec, F. Kadlec, P. Kuzel, K. Blary, P. Mounaix, Materials analysis by terahertz spectroscopy, *Opt. Lett.*, **33** (2008) 396–398.

[15] B. Sartorius, H. Roehle, H. Künzel, et al., All-fiber terahertz time-domain spectrometer operating at 1550 nm telecom wavelengths, *Opt. Express*, **16** (2008) 9565–9570.

[16] D.A.G. Bruggeman, Berechnung verschiedener physikalischer Konstanten von heterogenen Substanzen, *Ann. Phys.*, **416** (1935) 636–664.

[17] T. Iida, S. Nozaki, T. Takahashi, H. Kayanuma, Terahertz time-domain spectroscopy of TiO_2 nanoparticles, *J. Appl. Phys.*, **103** (2008) 084906.

[18] E. Hendry, M. Koeberg, B. O'Regan, M. Bonn, Local field effects on electron transport in nanostructured TiO_2 revealed by terahertz spectroscopy, *Nano Lett.*, **6** (2006) 755–759.

[19] K.P. Loh, S.W. Tong, J. Wu, Graphene and graphene-like molecules: prospects in solar cells, *J. Am. Chem. Soc.*, **138** (2016) 1095–1102.

[20] G.M. Turner, M.C. Beard, C.A. Schmuttenmaer, Carrier localization and cooling in dye-sensitized nanocrystalline titanium dioxide, *J. Phys. Chem. B*, **106** (2002) 11716–11719.